

Structure and thermodynamics of anisotropic polymer fluids

Galen T. Pickett

Department of Physics and Astronomy, California State University, Long Beach, 1250 Bellflower Blvd., Long Beach, California 90840

Kenneth S. Schweizer^{a)}

Departments of Materials Science & Engineering and Chemistry, and Materials Research Laboratory, University of Illinois, 1304 W. Green St., Urbana, Illinois 61801

(Received 2 August 1999; accepted 17 December 1999)

We investigate the structure and thermodynamics of anisotropic polymer fluids, focusing on the nematic phases of flexible polymers. The chains interact only through monomer–monomer excluded-volume interactions. As a function of an externally provided alignment along a fixed nematic director, we calculate the anisotropic pair correlation function, and demonstrate the existence of two density correlation lengths, ξ_{\perp} and ξ_{\parallel} , controlling transverse and longitudinal density fluctuations, respectively. We allow the possibility that the chains align either along the director (nematic conformations), or are anti-aligned in a “discotic-like” configuration. The cohesive contribution to the free energy is established in a high-temperature approximation, and its sensitivity to the orientation of the chains is probed. Our approach is not limited to homogeneous liquid crystalline phases, but applies in any circumstance when the *orientation* of otherwise disordered polymers is the physically controlling effect, e.g., confinement in thin films or pores, shear-alignment of flexible polymers, or straining a cross-linked rubber network. © 2000 American Institute of Physics. [S0021-9606(00)51410-X]

I. INTRODUCTION

Anisotropy is the key physical feature in many important complex fluid applications, especially in those of polymer liquid crystals.¹ The simplest case is that of the *nematic* phase, displaying only orientational order along a director.² This phase is triggered through concentrating a solution (lyotropic transition) or through cooling a melt (thermotropic transition), and represents a subtle compromise between reducing excluded-volume interactions, decreasing orientational entropy, and increasing cohesive contacts. Nematic phases (and liquid crystal phases in general) possess important physical properties as a result of this partial ordering: enhanced strength, anisotropic optical response, improved melt processing, and fast switching.

Another situation in which anisotropy is key is in processing of polymers, polymer blends, and in the shearing of polymer solutions.³ The shear field stretches the chains along the direction of the flow.⁴ This change of conformation has thermodynamic consequences which are not yet fully understood, sometimes raising and sometimes lowering the critical temperature of a solution.^{5–7} Polymers inhabiting explicitly anisotropic media are also important technologically. Uncrosslinked polymer in a stretched rubber network experience the anisotropy of the matrix polymers, and adopt an alignment similar to that imposed on the matrix chains.⁸

Also, engineered additives invading a polymer brush act in a markedly anisotropic environment.⁹ These brushes are designed as lubrication enhancing layers,¹⁰ compatibility enhancers at the surface of colloids,⁹ and to control the bio-

activity of viral particles.¹¹ Self-assembled versions appear when diblock copolymers undergo a microphase separation transition, or at the interface between incompatible polymer domains.^{3,12} These model *membranes* can be thought of as mimicking important features of a phospholipid bilayer.¹³ The question of how additive molecules pass through the brush, and their thermodynamics in the system, are the keys to understanding and controlling drug delivery in liposomes,¹⁴ and globular protein function in cell membranes.¹⁵ The *anisotropy* of the membrane the additives inhabit is a key physical feature.

Confining polymer films between two surfaces is also a situation of considerable anisotropy.⁹ Confinement (on a scale large compared to a monomer size, but small compared to the chain radius of gyration) forces the chains to adopt anisotropic conformations, with entropic and enthalpic consequences. The confusing behavior of the glass transition temperature of confined melts¹⁶ (certainly a dynamic effect), and the rise or fall of the miscibility of a confined fluid, are thus related through the *anisotropy* enforced by the confining interfaces.¹⁷

In these situations, anisotropy appears for different reasons (thermodynamic, external forcing, or confinement). Independent of the source of anisotropy, the *degree* of anisotropy can be treated as a phenomenologically (indeed, operationally) fixed parameter. Thus, the consequences of a fixed anisotropy on the polymer *fluid structure* is important to explore. We undertake this task below in a unified framework whose natural focus is the anisotropic liquid structure of aligned fluids,¹⁸ the microscopic polymer reference interaction site model (PRISM)¹⁹ based on the Chandler–Andersen RISM theory of small, rigid molecules.²⁰ Under its

^{a)}Electronic mail: kschweiz@uiuc.edu

anisotropic generalization, PRISM is naturally able to address questions of structure and thermodynamics in oriented fluids. We set out first to describe anisotropic PRISM with the physically reasonable, but much simplified “thread” polymer model.²¹ Here, the polymers have only excluded volume interactions at contact, and the chains are completely flexible. We then extend the range of the excluded volume interactions so that the monomer sites occupy a finite volume, with a close-packed, incompressible state in their isotropic phase. In this paper, we are solely interested in deducing the structural and thermodynamic consequences of maintaining the chains with a fixed, externally determined, anisotropy. This information is a foundation for more detailed thermodynamic treatments, and is crucial input to microscopic theories of dynamics in anisotropic polymer fluids.²²

Section II briefly reviews PRISM and the thread model in the isotropic phase, and introduces the “cutoff-thread” closure. Section III presents the anisotropic version of PRISM for aligned, but unstretched, flexible polymers. A brief account of the formalism, and its application to liquid crystallinity in thread polymers, has been recently published as a rapid communication.¹⁸ The thermodynamics of cutoff-thread polymers held at a fixed alignment is presented. Expressions for the isothermal compressibility and the equation of state are derived. In Sec. IV, the model predictions for structural and cohesive properties are described. Extensions to liquids composed of general mass-fractals are discussed in Sec. V, and a brief application of the formalism is presented that predicts an enhanced miscibility for thin-film polymer blends. We then draw our conclusions. In the following companion paper, we apply the formalism to the lyotropic transitions of flexible polymers.²³

II. ISOTROPIC PRISM

For long chain homopolymers composed of equivalent sites (alternatively monomers, or segments), the central goal is to determine the site–site intermolecular pair-correlation function, $g(\mathbf{r})$. The chain architecture and the number density of sites, ρ , together determine $g(\mathbf{r})$. The chain architecture is encoded in the single-chain pair correlation, $\omega(\mathbf{r})$, or its Fourier transform, the single-chain scattering function, $\omega(\mathbf{q})$. For flexible ideal Gaussian polymers characterized by a single statistical segment length, σ_o , $\omega(\mathbf{q})$ is the familiar Debye function, which we approximate conveniently with the standard Lorentzian form^{21,24}

$$\omega(\mathbf{q}) = \frac{N}{1 + (N\sigma_o^2/12)\mathbf{q} \cdot \mathbf{q}}. \quad (1)$$

Here, the chain is composed of N segments with radius of gyration $R_g^2 = N/6\sigma_o^2$. This dependence on \mathbf{q} approximates the true Debye function²⁵ to within 10% across the full range of q . Also, $\omega(\mathbf{q})$ is a function of $|\mathbf{q}|$ alone, as is appropriate for the description of a disordered, isotropic system of flexible polymers.

A. Thread model

The PRISM equation describing the propagation of correlations is

$$h(\mathbf{q}) = \omega(\mathbf{q})C(\mathbf{q})\omega(\mathbf{q}) + \rho h(\mathbf{q})C(\mathbf{q})\omega(\mathbf{q}), \quad (2)$$

where $h(\mathbf{r}) = g(\mathbf{r}) - 1$, and $C(\mathbf{q})$ is the interchain site–site direct correlation function. The thread model²¹ consists of a “core” exclusion condition that $g(\mathbf{r}=0) \equiv 0$, and a closure approximation that $C(\mathbf{r}) = c_o \delta(\mathbf{r})$. In wave-vector space:

$$C(\mathbf{q}) = c_o, \quad \text{and} \quad \int \frac{d\mathbf{q}}{(2\pi)^3} h(\mathbf{q}) \equiv -1. \quad (3)$$

c_o is chosen to satisfy the core condition. Thus, exclusion is enforced, and direct correlations are propagated, only at *contact*. The true direct correlation function of nonzero thickness polymers has a spatial range of the order of the monomer diameter, d . $C(\mathbf{q})$ vanishes for $|q| \gg 1/d$, and $g(\mathbf{r}) = 0$ for all $|r| < d$. Thus, the thread model is the “small d ” limit of the Percus–Yevick (PY) closure.^{19,20,26,27} Taking $d \ll \sigma_o$ is the limit which justifies the thread model. Since d is a *chemical*, or monomer, length-scale rather than a collective, statistical one (like σ_o) we expect this limit to be a “universal” regime controlled by chain dimensions and interpenetration, not local chemical detail.²⁵ Indeed, the full PY closure for the PRISM description of flexible, nonzero thickness athermal Gaussian chains has recently been solved *exactly* by Fuchs.²⁸ The analytic solution for $d \neq 0$ reduces exactly to the PRISM thread predictions for dilute and semidilute densities.^{25,29}

The thread model can be analytically solved^{19,21}

$$c_o^{\text{thread}} = -\frac{\pi\sigma_o^3}{\sqrt{27N}} - \frac{\pi^2\rho\sigma_o^6}{108}. \quad (4)$$

From this, a range of useful structural information can be calculated. For example, the function describing the total collective density fluctuations is the static structure factor, $S(\mathbf{q})$, given by

$$S(\mathbf{q}) = \omega(\mathbf{q}) + \rho h(\mathbf{q}) \equiv \frac{S_o}{1 + \xi^2 q^2}, \quad (5)$$

where the second equality is exact under our Lorentzian approximation for $\omega(\mathbf{q})$, Eq. (1), and the pointwise nature of direct correlations, Eq. (3). The dimensionless isothermal compressibility, $S_o = S(\mathbf{q}=0) \equiv \rho k T \kappa_T$, with κ_T the true isothermal compressibility, appears in Eq. (5). Below, we adopt thermal energy units, that is $kT = 1$ (Boltzmann’s constant multiplied by the temperature). The density fluctuation screening length, ξ , is defined in Eq. (5). In terms of the direct correlation parameter, c_o

$$S_o = \frac{1}{(1/N) - \rho c_o}, \quad (6)$$

$$\xi = \frac{\sigma_o}{2\sqrt{3}} \frac{1}{\sqrt{(1/N) - \rho c_o}}. \quad (7)$$

This relationship between S_o, ξ , and c_o holds for all pointwise closures, not just the thread. When the explicit expression for c_o^{thread} is employed, one has:

$$S_o^{\text{thread}} = \left(\frac{1}{\sqrt{N}} + \frac{\pi \rho \sigma_o^3}{6\sqrt{3}} \right)^{-2} \approx \frac{108}{\pi^2 \sigma_o^2 \rho}, \quad N \rightarrow \infty, \quad (8)$$

$$\xi^{\text{thread}} = \frac{\sigma_o}{2\sqrt{3}[(1/\sqrt{N}) + (\pi \rho \sigma_o^3/6\sqrt{3})]} \approx \frac{3}{\pi \sigma_o^2 \rho}, \quad N \rightarrow \infty, \quad (9)$$

where we note the $N \rightarrow \infty$ limit. The universal semidilute scaling²⁵ of the screening (or ‘‘blob’’) length is recovered: $\xi \sim (\sigma_o^2 \rho)^{-1}$.

B. Thread with wavevector cutoff

Extending the thread model beyond the universal regime requires the length scale d . A simple approximation scheme to account for $d \neq 0$ within a threadlike context is the so-called ‘‘string’’ closure (or model).^{19,21} One retains the pointwise nature of direct correlations, but chooses the direct correlation parameter c_o to enforce an average exclusion constraint: $\int_0^d r^2 dr g(\mathbf{r}) \equiv 0$. This formulation can be justified as an optimized perturbation theory about a thread reference.²¹ The model agrees with the thread in the universal regime. The string model fluid pressure diverges at $\rho = 9(2\pi\sigma_o^2 d)^{-1}$, which may be associated operationally (but not rigorously) with a close-packed, incompressible arrangement of the excluding sites.³⁰

One technical problem with the string closure is that it fails to *a priori* guarantee $g(\mathbf{r}) > 0$ for $r > d$. For isotropic fluids where $g(\mathbf{r}) = g(|\mathbf{r}|)$, the string model indeed produces a positive definite pair correlation for all, $r > d$. As discussed in the following companion paper,²³ when $g(\mathbf{r})$ is explicitly anisotropic it is possible for $g(r)$ to remain negative in some directions as \mathbf{r} moves outside the exclusion sphere.

An alternative threadlike closure which rigorously avoids this problem is motivated by the structure of the exact direct correlation function. For both simple fluids²⁶ and isotropic polymeric fluids,¹⁹ $C(\mathbf{q})$ is an oscillating function, initially negative, whose first zero occurs at the scale $q \approx \pi/d$. To mimic in the simplest possible manner this decay to zero of $C(\mathbf{q})$, we employ the physically reasonable ansatz:

$$C(\mathbf{q}) = c_o, \quad \text{when } q < q_c \equiv \frac{\pi}{d} \\ = 0, \quad \text{when } q > q_c. \quad (10)$$

Equation (10) with a pointwise exclusion constraint defines the ‘‘cutoff-thread’’ model. In the large N limit the exclusion constraint $[\int d\mathbf{q} (2\pi)^{-3} h(\mathbf{q}) \equiv -1]$ becomes

$$\tanh \frac{\pi^2 \sqrt{\rho} \sigma_o^3}{12\sqrt{3}c_o} = \frac{\pi \sigma_o}{2d\sqrt{3}c_o \rho}. \quad (11)$$

Using Eq. (6), the direct correlation parameter c_o can be eliminated in favor of the *directly measurable* correlation

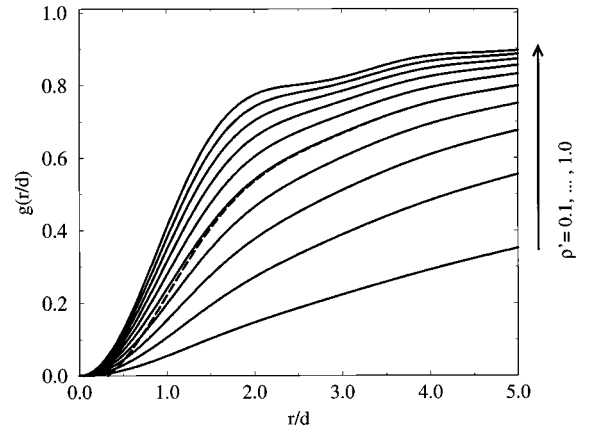


FIG. 1. The isotropic $g(r)$ from the cutoff thread model for reduced density, $\rho' = 0.1, \dots, 1.0$ in increments of 0.1. As ρ' approaches its maximal value, weak ‘‘solvation’’ shells appear. The dashed line is for $\rho' = 0.5$ based on the approximate closure discussed in Sec. II C.

length, ξ . When we use dimensionless quantities, $\xi' \equiv \xi/d$ and $\rho' \equiv \pi \rho d \sigma_o^2 / 6$, the exclusion constraint becomes

$$\pi \xi' \rho' = \arctan \pi \xi'. \quad (12)$$

Significantly, when $\rho' = 1$, the solution to Eq. (12) is $\xi' = 0$, that is the compressibility of the fluid vanishes. Thus, the cutoff-thread model captures a maximal density, close-packed situation when the monomer density is

$$\rho_{\text{max}} = \frac{6}{\pi d \sigma_o^2}. \quad (13)$$

We have thus chosen the density of this close-packed state to be the scale of density in our arguments below. Modification of the cutoff wavenumber in Eq. (10) by a numerical factor ($q_c \rightarrow b q_c$) simply rescales all the above results by $d \rightarrow d/b$.

Figure 1 shows results for $g(\mathbf{r})$ based on the cutoff-thread model implemented numerically. As $\rho' \rightarrow 1$ weak ‘‘solvation’’ shells develop. The high-wavevector dependence of the full direct correlation function is responsible for developing the characteristic solvation structure of high-density fluids.²⁶ Providing $C(\mathbf{q})$ with the trivial step-function dependence at $|\mathbf{q}| = \pi/d$ is enough to allow the simple thread model to crudely capture this feature. It is important to note, however, that the periodicity of the solvation shells is approximately twice that expected from the packing of d -sized spheres, and is clearly sensitive to the precise location chosen for the cutoff. If in Eq. (10) we choose $C(\mathbf{q})$ to be cutoff at $|\mathbf{q}| = b\pi/d$, then the r in Fig. 1 should be scaled by d/b , where we expect the ‘‘best’’ b for a specific polymer to be a number of order unity. With $b = 2$, the characteristic periodicity of the solvation shells in Fig. 1 becomes $\approx d$. Interestingly, at high densities the contact value of the pair correlation function $[g(r=d)]$ saturates at ~ 0.4 , a value typical of real molten (but compressible) flexible polymers.^{19,31}

Choosing ξ' in accordance with Eq. (12) ensures the *positivity* of $g(\mathbf{r})$. The pointwise condition ensures that $g(\mathbf{r}=0) \equiv 0$, and it is a simple matter to prove that $g(\mathbf{r})$ is an increasing function of r . Significantly, this is true also for the

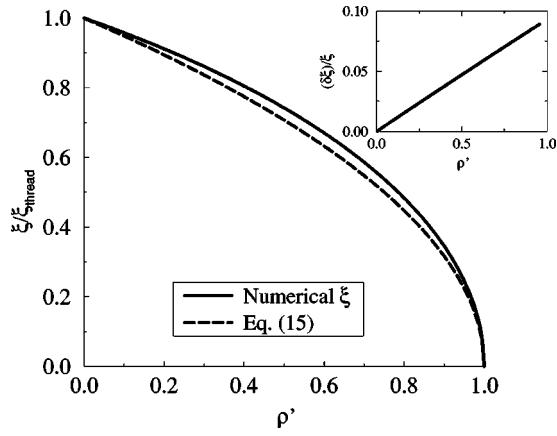


FIG. 2. Approximate vs exact cutoff closure. ξ derived from the exact numerical solution of the cutoff model is shown as the solid curve, scaled by the thread model screening length, ξ^{thread} . The dashed line shows the same quantity derived from Eq. (15). The inset shows the relative error incurred: $(\delta\xi)/\xi$, where $\delta\xi$ is the difference between the exact and interpolated ξ' . The error increases linearly up to a maximal value of 8%.

anisotropic phases discussed below. While the string closure requires $g(\mathbf{r}) < 0$ for at least some $r < d$, the cutoff-thread closure maintains a positive pair correlation function for all \mathbf{r} . Additionally, for small r , $g(\mathbf{r}) \sim r^2$, so that the pair correlation vanishes quadratically.

C. Interpolated closure

When $\rho' \ll 1$ in the closure relation, Eq. (12), the universal “semidilute” scaling regime of polymer physics, and the results of the thread model are recovered. If we scale $\xi'(\rho')$ [obtained by numerically solving Eq. (12)] by its asymptotic semidilute thread behavior, one naturally obtains a quantity bounded by 1 as $\rho' \rightarrow 0$, and which vanishes at $\rho' = 1$, as shown in Fig. 2 (solid line). It is a simple matter to deduce the manner in which $\xi'(\rho')$ vanishes

$$\xi' = \frac{\sqrt{3(1-\rho')}}{\pi} + O[(1-\rho')]. \quad (14)$$

A suitable analytic interpolation between the universal behavior, Eq. (9), and the concentrated, incompressible behavior, Eq. (14), is given by

$$\xi' = \frac{\sqrt{1-\rho'}}{2\rho'}. \quad (15)$$

This approximate screening length (again, normalized by the thread result) is shown as the dashed line in Fig. 2, and the inset shows the relative error between Eq. (15) and the exact numerical cutoff thread closure. As “engineered,” the results match closely for $\rho' \rightarrow 0$, and diverge slightly (by less than 10% at $\rho' = 1$). We have checked that the liquid structure, $g(\mathbf{r})$, based on the interpolated closure closely approximates that of the numerically exact calculations. $g(\mathbf{r})$ differs the most from its numerically exact value near $\mathbf{r} = 0$, where its deviation is approximately equal to the relative error shown in the inset to Fig. 2. The deviation of the approximate closure from the exact numerical result implies that $g(\mathbf{r})$ fails to vanish at $\mathbf{r} = 0$, sometimes taking (weakly) posi-

tive or negative values. However, the ease of calculations based on Eq. (15) justifies its use, as well as the physically reasonable results that follow from it. It should be noted that the entire basis of this discussion is the Lorentzian form for $\omega(\mathbf{q})$, which itself deviates from the “exact” form of the Gaussian chain Debye function by as much as 10%. The dashed line in Fig. 1 shows $g(\mathbf{r})$ as determined from the approximate, interpolated closure, Eq. (15) for $\rho' = 0.5$. There is good agreement between the numerically exact and interpolated $g(\mathbf{r})$'s.

III. ANISOTROPIC PRISM

With the theoretical tools above, we construct a liquid-state description of anisotropic macromolecular liquids. A large class of anisotropic polymer fluids can be modeled by the following choice of single-chain structure factor:

$$\omega(\mathbf{q}) = \frac{N}{1 + (N/4) q_a q_b \sigma_{ab}}, \quad (16)$$

where the repeated roman indices imply summation over the cardinal directions, (x, y, z) . Here, σ_{ab} is a symmetric tensor that determines the specific physical situation of interest. This form of $\omega(\mathbf{q})$ describes an *anisotropic* random walk; that is, an ideal random walk with different step lengths σ_{ab} in different directions. With the choice

$$\sigma_{ab} = \delta_{ab} \sigma_a^2, \quad (17)$$

$$\sigma_x = \frac{\sigma_o}{\sqrt{\lambda}}, \quad (18)$$

$$\sigma_y = \frac{\sigma_o}{\sqrt{\lambda}}, \quad (19)$$

$$\sigma_z = \lambda \sigma_o, \quad (20)$$

Eq. (16) describes a stretched polymer subjected to a uniaxial strain of magnitude λ in the \mathbf{z} direction, embedded in a homogeneous, incompressible material.²⁵ We could repeat all that follows with this choice of ω , and indeed many others.

A judicious choice of σ_{ab} for studying the *alignment* rather than the *stretching* of polymer chains is

$$\sigma_{ab} = \delta_{ab} \sigma_a^2, \quad (21)$$

$$\sigma_x = \sigma_y \equiv \sigma_{\perp} = \sigma_o \frac{\sqrt{1-\tau}}{\sqrt{3}}, \quad (22)$$

$$\sigma_z = \sigma_o \frac{\sqrt{1+2\tau}}{\sqrt{3}}. \quad (23)$$

Clearly, a random walk described by such a σ_{ab} has the *same* radius of gyration³² as the isotropic chain, since $\sigma_x^2 + \sigma_y^2 + \sigma_z^2 = \sigma_o^2$. Simultaneous *orientation* and *stretching* of the polymers can be described by combining λ and τ .

It is clear that τ is the usual nematic order parameter.¹ Inverting Eq. (23): $\tau = (3\sigma_z^2/\sigma_o^2 - 1)/2$ where the alignment angle θ of the “bond” connecting sites is $\langle \cos^2 \theta \rangle^{1/2} = \sigma_z/\sigma_o$ as in the schematic, Fig. 3. The sign (magnitude) of the nematic order parameter, τ , marks the type (degree) of alignment. When $\tau = 0$, one has isotropic flexible coils. Nem-

atic configurations are characterized by $\tau > 0$, in which the chain random walk is longer along the nematic director \hat{z} than perpendicular to the director. The opposite case holds for $\tau < 0$. Here the chains adopt *dislike* conformations, spread out in the plane perpendicular to the director, and compressed along it. While we shall refer to $\tau < 0$ as a ‘‘discotic’’ phase, the chains are homogeneously distributed in space, and are not allowed to arrange themselves in the columns characteristic of true discotic liquid crystals.¹

The many chain problem is treated with the same PRISM formalism sketched in Sec. II [Eqs. (2),(3), and (10)]. The cutoff thread PY closure of Eq. (10) assumes that the direct correlation function vanishes in an isotropic manner, that is for $|\mathbf{q}| > q_c$, independent of the orientation of the chains. Thus, the monomer sites on an aligned chain are still assumed to exclude monomers from their spherical, isotropic exclusion volume, and influence neighboring interchain monomers with a contact range on the order of d , again isotropically distributed. The anisotropy enters *only* in the global chain dimensions through $\omega(\mathbf{q})$ and σ_{ab} .

A. Anisotropic thread results

It is instructive to review the implications of the PRISM equation with Eqs. (21)–(23) in the literal thread limit, $d \rightarrow 0$, or equivalently, when the wave-vector cutoff in Eq. (12) becomes indefinitely large.¹⁸ In direct analogy to the isotropic thread results above, the collective structure factor is:

$$S(\mathbf{q}) \equiv \frac{S_o(\tau)}{1 + q_{\perp}^2 \xi_{\perp}^2 + q_z^2 \xi_z^2}. \quad (24)$$

The dimensionless compressibility gains a τ -dependence, but even more striking is the anisotropic form of the screening of density fluctuations. These fluctuations are governed by ξ_{\perp} lateral to the director’s axis, and by ξ_z along it. After executing the analytic thread closure for finite degree of polymerization, N , one obtains¹⁸

$$S_o^{\text{thread}} = \left(\frac{1}{\sqrt{N}} + \frac{\pi \rho \sigma_o^3 (1 - \tau) \sqrt{1 + 2\tau}}{6\sqrt{3}} \right)^{-2}, \quad (25)$$

$$\xi_z^{\text{thread}} = \left(\frac{\pi \rho \sigma_o^2 (1 - \tau)}{3} + \frac{2\sqrt{3}}{\sqrt{N} \sigma_o \sqrt{1 + 2\tau}} \right)^{-1}, \quad (26)$$

$$\xi_{\perp}^{\text{thread}} = \left(\frac{\pi \rho \sigma_o^2 \sqrt{(1 - \tau)(1 + 2\tau)}}{3} + \frac{2\sqrt{3}}{\sqrt{N} \sigma_o \sqrt{1 - \tau}} \right)^{-1}. \quad (27)$$

These expressions are valid in the *thread* limit only, and not at finite d . Clearly, at either full nematic alignment ($\tau = 1$) or at full discotic alignment ($\tau = -1/2$), S_o^{-1} falls to its lowest value, that of an ideal solution of objects composed of N monomers. In the $N \rightarrow \infty$ limit, S_o^{-1} vanishes at full nematic or discotic alignment. This is in keeping with the requirement that N enters as a well-controlled, finite-size correction to the universal, $N \rightarrow \infty$ limit. $S_o(\tau)$ describes the influence of excluded volume interactions on the long-wavelength density fluctuations of the system, and increasing $|\tau|$ shrinks the

invaded space of each chain, so that neighboring chains overlap less. Interestingly, ρ appears in S_o with a particular combination of τ and N . Through the definition $\rho^*(\tau) \equiv (\sqrt{N} \sigma_z \sigma_{\perp}^2)^{-1}$, the thread-level compressibility assumes a simple form

$$S_o^{\text{thread}} = \frac{1}{N} \left(1 + \frac{\pi \rho}{2 \rho^*} \right)^2. \quad (28)$$

Clearly, $\rho^*(\tau)$ is proportional to the *anisotropy-dependent* semidilute overlap threshold density of chains held at a constant τ . Each chain covers a volume $\approx R_z R_{\perp}^2 \approx N^{3/2} \sigma_z \sigma_{\perp}^2$, and contains N monomers. Thus, the internal density of monomers inside an isolated coil is $\approx N / (R_z R_{\perp}^2) \sim \rho^*(\tau)$. S_o takes on a simple scaling form in the pure thread theory, consistent with the anisotropic version of the standard scaling hypothesis of polymer physics.²⁵ It is a simple matter to employ Eq. (28) and arrive at the anisotropic semidilute forms of thermodynamic properties.¹⁸ The equation of state, for example, is

$$\begin{aligned} \frac{P}{kT} = \frac{\rho}{N} + \frac{\pi \sqrt{3} \sigma_o^3 (1 - \tau) \sqrt{1 + 2\tau}}{18 \sqrt{N}} \rho^2 \\ + \frac{\pi^2 \sigma_o^6 (1 - \tau)^2 (1 + 2\tau)}{324} \rho^3. \end{aligned} \quad (29)$$

At the thread level, up to the third virial contribution in the equation of state is captured. At the very smallest densities, the ideal gas pressure of the isolated polymer chains (ρ/N) is recovered. Both the latter and second virial contributions become irrelevant as $N \rightarrow \infty$, thereby yielding a universal semidilute pressure law, $P \sim (\rho \sigma_o^2)^3$, but with an anisotropy-controlled prefactor.

B. Nonzero thickness model

At least in the isotropic, athermal case, the string closure and the cutoff closure are complimentary, and choosing between them has no influence upon the qualitative features of results. The string closure enforces an average exclusion volume per site, but maintains the pointwise nature of direct correlations. The cutoff closure extends the range of the direct correlations, but maintains exclusion only at a single point. Both models predict an incompressible state, and in the small density limit yield the thread model; thus, the analytic interpolation for both the string and the cutoff

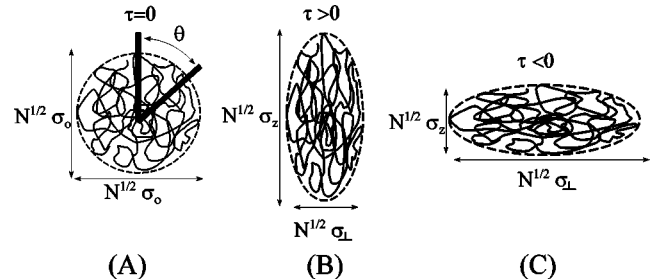


FIG. 3. Schematic. (A) typical isotropic phase configuration for a single, random walk chain. (B) Nematic configuration, where the chain takes longer steps along the \hat{z} direction than lateral to it ($\tau > 0$). (C) Discotic configuration ($\tau < 0$).

models is of the same form, and differs merely by a numerical prefactor. However, in the anisotropic phases, the cutoff model is clearly superior, as it maintains $g(\mathbf{r}) > 0$ in all physical regions of the model. Thus, structural quantities related to dynamics (for example, the contact value of the pair correlation), and thermodynamic perturbation estimates of the liquid cohesion, will be best described by our novel cutoff thread closure, or indeed, the analytically tractable interpolation scheme we derive below.

Given the choice of $\omega(\mathbf{q}; \tau)$ above, one can devise an approximate, interpolated closure along the lines of that presented in Eq. (15). Specializing to the $N \rightarrow \infty$ case yields:

$$\omega(\mathbf{q}; \tau) = \frac{12}{q^2 \sigma_o^2 (1 - \tau + 3\tau u_\theta^2)}, \quad (30)$$

$$h(\mathbf{q}; \tau) = -\frac{2d\pi}{q^2 \rho' (1 - \tau + 3\tau u_\theta^2)} \times (1 + [\xi' q d]^2 (1 - \tau + 3\tau u_\theta^2) \rho')^{-1}, \quad (31)$$

$$S(\mathbf{q}; \tau) = 12 \left[\frac{\xi' d}{\sigma_o} \right]^2 (1 + [\xi' d q]^2 (1 - \tau + 3\tau u_\theta^2))^{-1}. \quad (32)$$

Here we have adopted spherical coordinates for the wavevectors, $\mathbf{q} = (|\mathbf{q}|, u_\theta, \phi)$, where $u_\theta = q_z/q$ is the azimuthal cosine. We have eliminated the unknown c_o in favor of the equally unknown screening length, ξ' . Solving the model thus means giving a prescription for the value of ξ' . Clearly, all the major structural properties of a fluid with a nonzero τ are themselves anisotropic. We define ξ' and ρ' to coincide with their definitions in the isotropic case. As noted above, in the anisotropic phase, there are *two* density screening lengths, parallel and perpendicular to the director

$$\xi'_z = \xi' \frac{\sigma_z}{\sigma_o \sqrt{3}} = \xi' \sqrt{1 + 2\tau}, \quad (33)$$

$$\xi'_\perp = \xi' \sqrt{1 - \tau}. \quad (34)$$

These definitions preserve the thermodynamic relation between the dimensionless compressibility and the screening length:

$$S_o^{-1} = \frac{1}{12} \left[\frac{\sigma_o}{\xi' d} \right]^2. \quad (35)$$

ξ' is thus an appropriate ‘‘isotropization’’ of the anisotropic screening lengths.

The core condition to apply in this model is:

$$\int_0^{\pi/d} dq \int_{-1}^1 du_\theta \frac{q^2}{4\pi^2} h(\mathbf{q}; \tau) \equiv -1, \quad (36)$$

for which there is no general, analytic solution. In the thread limit ($d \ll \sigma_o$, and large ξ') we can recover the *anisotropic* thread result from Eq. (36):

$$\xi'_{\text{thread}} = \frac{1}{2\rho' (1 - \tau) \sqrt{1 + 2\tau}}. \quad (37)$$

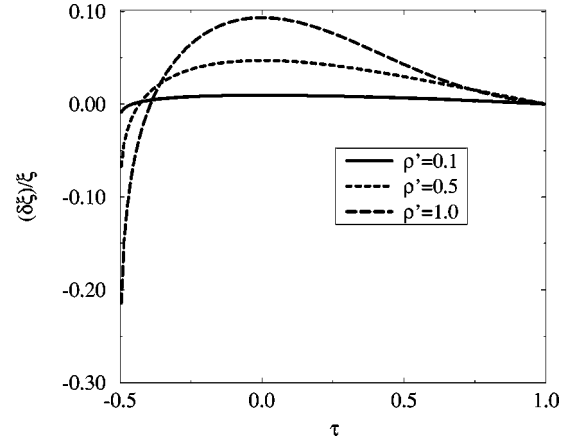


FIG. 4. Approximate anisotropic closure. The relative error incurred by the interpolated closure for the cutoff thread model in the anisotropic phases is shown as a function of τ . The reduced densities are as labeled in the plot. For small density, in the semidilute regime, the error is small across the entire range of τ , reaching a maximal relative value of less than 1% at full discotic alignment. The approximation gets worse as $\rho' \rightarrow 1$, saturating at nearly a 20% error in the discotic phases.

In the dilute limit, the ξ' diverges as $1/\rho'$ [compare to Eq. (7)]. At the other extreme in ρ' , ξ' vanishes at a τ -dependent density

$$\xi' = \frac{\sqrt{3}}{\pi} \sqrt{\rho'_{\text{max}}(\tau) - \rho'}, \quad (38)$$

where

$$\rho'_{\text{max}}(\tau) = \frac{1}{\sqrt{3\tau(1-\tau)}} \arctan \sqrt{\frac{3\tau}{1-\tau}}. \quad (39)$$

Thus, a semianalytic form which approximates the closure relation, Eq. (36), is

$$\xi'(\tau) = \frac{\sqrt{1 - [\rho'/\rho'_{\text{max}}(\tau)]}}{2\rho' (1 - \tau) \sqrt{1 + 2\tau}}. \quad (40)$$

As in the isotropic phase ($\tau=0$, Fig. 2), we may ask how numerically accurate this approximate closure is. Figure 4 shows the relative error incurred at $\rho' = 0.1, 0.5, 1.0$. As is evident, for meltlike and semidilute densities, $\rho' < 0.5$, this approximation reproduces the exact solution to Eq. (36) to within 10%. At the maximum isotropic phase density, Eq. (40) is weakest in the extreme discotic phase, that is near $\tau = -0.5$, where the error becomes as large as 20%. Thus, one may expect some discotic-phase errors in any calculation based on Eq. (40) near full alignment. Most of our detailed results below are based on this interpolation of the cutoff model closure. The error incurred by this interpolation affects the numerical value of $g(\mathbf{r})$ in the anisotropic phases. The deviation (not shown) between the numerically exact and the interpolated pair correlation functions is greatest at $\mathbf{r}=0$, and quickly vanishes when r exceeds a few σ_o .

Figure 5 shows the behavior of the dimensionless isothermal compressibility as a function of τ for various densities, $\rho' = 0.1, \dots, 1.0$. In the approximation, Eq. (40), it is a simple matter to calculate the inverse dimensionless compressibility of a system of chains with τ held fixed

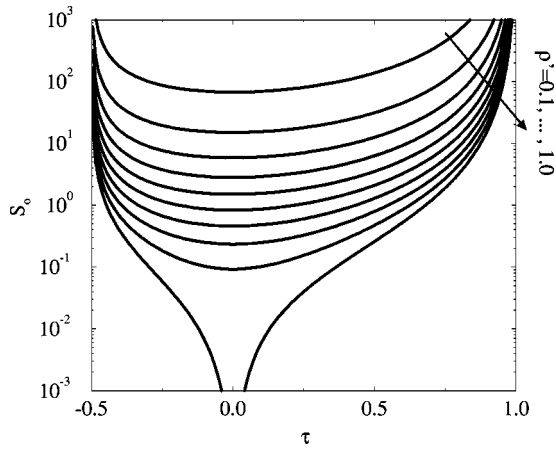


FIG. 5. S_o vs τ . The τ -dependent dimensionless compressibility for $\rho' = 0.1, \dots, 1.0$.

$$S_o^{-1}(\rho', \tau) = \left| \frac{\sigma_o \rho'}{d} \right|^2 \frac{\rho'_{\max}(\tau)(1-\tau)^2(1+2\tau)}{3(\rho' - \rho'_{\max}(\tau))}. \quad (41)$$

The choice of scaling variables, ξ', ρ' indicates that the dimensionless ratio (“aspect ratio”) σ_o/d appears in the compressibility only as a prefactor. As above, we have taken the limit $N \rightarrow \infty$ at the very beginning of the calculation. For any finite molecular weight, the value of S_o^{-1} cannot drop below N^{-1} , which is the dimensionless inverse compressibility associated with an ideal solution of N -monomer polymer chains. Therefore, while S_o really does *diverge* in the semi-log plot of Fig. 5 at both $\tau=1$ (perfect nematic alignment) and $\tau=-1/2$ (perfect discotic alignment), this is a consequence of the infinite molecular weight limit.³³ It is interesting to note that the curves for $\rho'=0.1-0.5$ are quite similar, indicating that the main effect of changing the site density ρ' is to determine the prefactor in a scaling function. This breaks down as $\rho' \rightarrow 1$, because, $S_o=0$ for unoriented chains at $\rho'=1$. Universality becomes untenable at high densities as local properties of the fluid become important.

Enhancement of the dimensionless compressibility by a small amount of chain alignment can be analytically determined by the small τ expansion of Eq. (40)

$$S_o = \frac{3d^2(1-\rho')}{4\sigma_o^2(\rho')^2} \left(1 + \frac{15-11\rho'}{5(1-\rho')} \tau^2 + \dots \right). \quad (42)$$

Each chain in the system sweeps out a smaller invaded volume when $|\tau|$ increases. That each chain overlaps with its neighbors *less* indicates that the system is behaving *more dilutely*. Hence, S_o increases, and the thermodynamic consequence of the chain–chain excluded volume interaction is lessened.

By employing the compressibility of the anisotropic fluid, one can determine the equation of state. Using standard thermodynamics (in an ensemble in which not only the temperature T but also τ is fixed), we have the usual “compressibility charging” formula

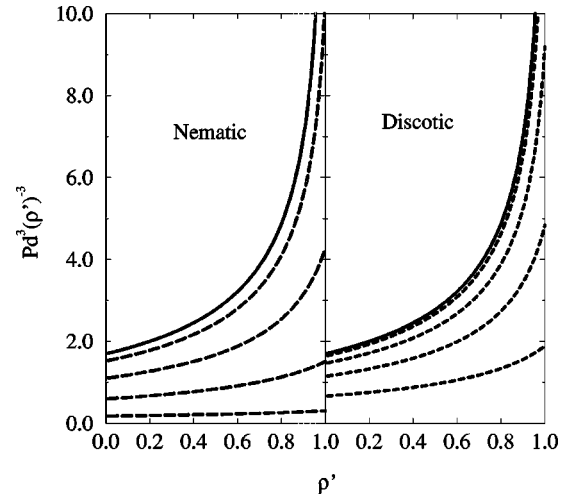


FIG. 6. Scaled pressure, $Pd^3(\rho')^{-3}$, at constant τ is plotted across the entire range of ρ' for various values of τ . The nematic values span $\tau = 0, 0.2, 0.4, 0.6, 0.8$, with the isotropic $\tau=0$ pressure plotted as a solid line. As τ increases, the pressure drops monotonically. $\tau=0, -0.1, -0.2, -0.3, -0.4$ in the discotic case.

$$P = \int_0^{\rho'} dx S_o^{-1}(x; \tau) = - \frac{8\rho'_{\max}(1-\tau)^2(1+2\tau)}{\pi d^3} \times \left((\rho')^2 + 2\rho'\rho'_{\max} + 2(\rho'_{\max})^2 \log \left[1 - \frac{\rho'}{\rho'_{\max}} \right] \right). \quad (43)$$

Thus, the isotropic-phase system has a *logarithmic* divergence in the pressure as $\rho' \rightarrow 1$, and allowing $\tau \neq 0$ negates this divergence by shifting it to a density greater than the isotropic fluid maximum density. As seen in Fig. 6, in both the nematic and discotic phases, the pressure is considerably *lessened* over that found in the isotropic fluid. Clearly, allowing the chains to adopt conformations such as those in Fig. 3 results in *fewer* pair-contacts, and hence the site–site excluded volume interaction has a weaker impact on the pressure.

Figure 7 shows the τ -dependence of P at various values of ρ' . In both the limits $\tau \rightarrow 1$ and $\tau \rightarrow -1/2$, the pressure vanishes. Again, the main variation in the pressure-vs- τ plots is to set the magnitude of a scaling function (shown clearly in the inset). The pressure is maximal near $\tau=0$, and falls away toward either the nematic or discotic configurations. As $\tau \rightarrow 1$, we have

$$P \approx \frac{16(\rho')^3(1-\tau)^2}{\pi d^3}, \quad (44)$$

and as $\tau \rightarrow -1/2$,

$$P \approx \frac{12(\rho')^3(1+2\tau)}{\pi d^3}. \quad (45)$$

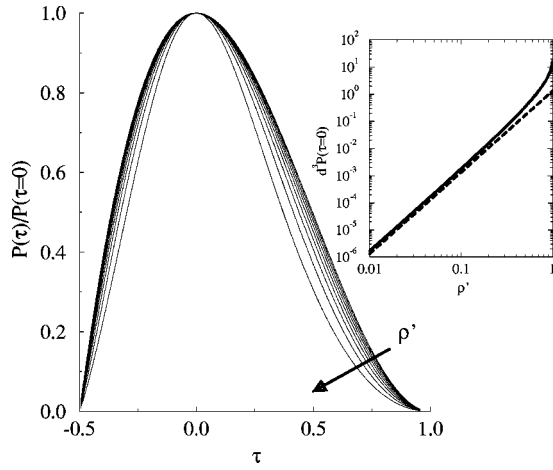


FIG. 7. The pressure scaled by its isotropic, $\tau=0$, value is plotted across the full range of τ , for various $\rho'=0.1, \dots, 1.0$. The shape of the equation of state is remarkably insensitive to ρ' for small ρ' indicating that the major effect of changing the density is to determine an overall scale factor. The dimensionless isotropic pressure, $P(\rho', \tau=0)d^3$ is shown in the inset, with a comparison to the semidilute power law (dashed line).

Thus, in *both* the discotic and nematic fully aligned systems, the liquid appears to display its *most dilute* form for its equation of state. That is, a *threadlike* behavior of the equation of state is recovered near full alignment.

IV. ANISOTROPIC LIQUID STRUCTURE AND COHESIVE ENERGY

Based on the approximate expression for $\xi'(\rho'; \tau)$, Eq. (40), one can easily study the liquid structure of the oriented fluid. As shown in Fig. 8 (for $N \rightarrow \infty$ chains), the parallel and perpendicular screening lengths in Eqs. (33) and (34) behave as expected. In the nematic region, the fluid has a much longer screening length along the director than perpendicular

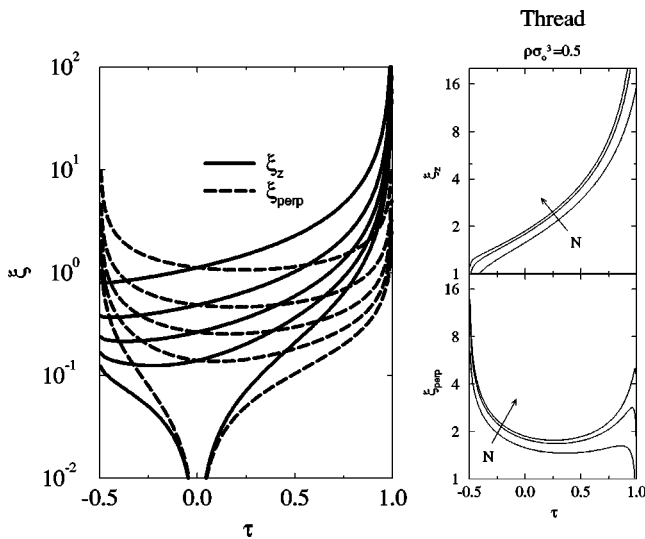


FIG. 8. ξ_z and ξ_\perp . We show the τ dependence of the dimensionless ξ_z (solid curves) and ξ_\perp (dashed curves) for various values of reduced density, $\rho'=0.2, \dots, 1.0$. In the nematic region, $\xi_z \gg \xi_\perp$. The opposite occurs for $\tau < 0$. The finite N behavior of both quantities is quite complicated, demonstrated by the thread-model predictions at finite $N=10^3, 10^4, 10^5$, shown to the right.

to it ($\xi_z' \gg \xi_\perp'$), and vice versa in the discotic phase. Anisotropy of density screening lengths plays an important role in determining the anisotropic transport properties of polymer fluids, especially for long chains where a strong correlation between ξ and entanglement length scale exists.²⁵ The finite- N behavior of these quantities is rather complicated, however. The largest ξ_z' can attain as $\tau \rightarrow 1$ scales as the radius of gyration: $\sigma_o N^{1/2}/2 = R_g 6^{1/2}/2$ (with the appropriate numerical prefactors inserted). In this limit, ξ_\perp' must vanish: $\xi_\perp' \approx N^{1/2} \sqrt{1-\tau}$. Similar statements may be made in the perfectly discotic arrangement ($\tau = -1/2$). Since, as in Eqs. (44) and (45), the approach to full alignment implies that threadlike results are recovered, the finite N behavior of cutoff-model thread polymers should be similar to that of the simple thread model as in Fig. 8.

These thread results are easy to obtain from Eqs. (26) and (27). Both anisotropic screening lengths, are bound above by $2^{-1/2} R_g \sim N^{1/2}$. Also, $\xi_z^{\text{thread}}(\tau = -1/2) = \xi_\perp^{\text{thread}}(\tau = 1) = 0$, implying that at full alignment the fluid cannot support lateral fluctuations in density. Thus, the fluid is *incompressible* laterally at full alignment. We note that even in the well-behaved thread model, taking the limit $N \rightarrow \infty$ can create spurious divergences in the directional screening lengths:

$$\xi_z^{\text{thread}} = \frac{3}{\pi \rho \sigma_o^2 (1-\tau)}, \quad \text{as } \tau \rightarrow 1, \quad (46)$$

$$\xi_\perp^{\text{thread}} = \frac{\sqrt{3}}{\pi \rho \sigma_o^2 \sqrt{1-\tau}}, \quad \text{as } \tau \rightarrow 1, \quad (47)$$

$$\xi_z^{\text{thread}} = \frac{2}{\pi \rho \sigma_o^2}, \quad \text{as } \tau \rightarrow -1/2, \quad (48)$$

$$\xi_\perp^{\text{thread}} = \frac{\sqrt{6}}{\pi \rho \sigma_o^2 \sqrt{1+2\tau}}, \quad \text{as } \tau \rightarrow -1/2. \quad (49)$$

These asymptotic behaviors are displayed in the cutoff model, as well. The true finite N behavior of ξ_\perp and ξ_z at saturated alignment cannot be deduced solely from the $N \rightarrow \infty$ limit. However, as $\tau \rightarrow 1$ or as $\tau \rightarrow -1/2$, the chain dimensions become more and more confined to a space of lower than three dimensions (one for nematic, two for discotic). Thus, the system returns to its *dilute* limit at full alignment, and we can be confident that the finite N thread results for $\xi_\perp^{\text{thread}}$ and ξ_z^{thread} adequately models the behavior in the cutoff model.

This finite- N behavior is not evident in the main section of Fig. 8. It does appear in the thread level results in the right panel of Fig. 8, which indicate the interesting behavior we can expect in a realistic finite N calculation. Here, results for ξ_z' and ξ_\perp' in the thread model are displayed for $N = 10^3, 10^4, 10^5$ and a site density of $\rho \sigma_o^3 = 0.5$. Clearly, the correct limiting behavior at $\tau = 1$ and $\tau = -1/2$ is found, and the inset suggest how the results in the main figure will be cutoff, so that ξ_\perp' does *not* diverge at $\tau = 1$, and ξ_z' does not approach a nonzero value at $\tau = -1/2$.

The anisotropic behavior of $g(\mathbf{r})$ can be determined numerically from inverse Fourier transforming $h(\mathbf{q})$ (not shown). The local correlation hole^{19,25} is found to be farther

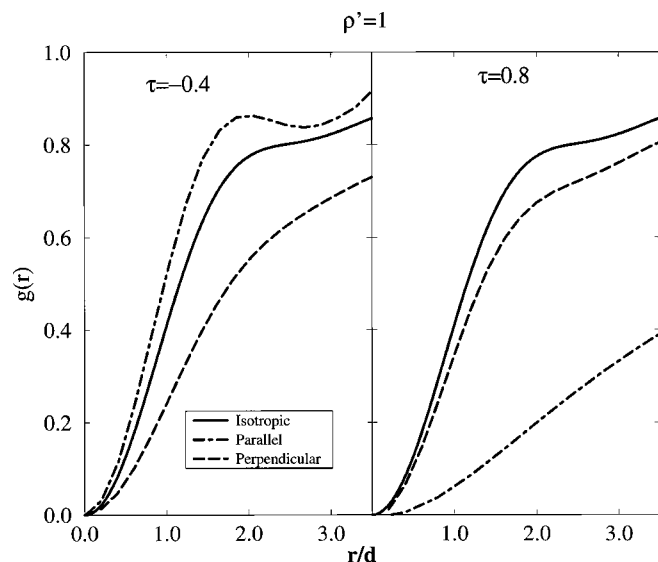


FIG. 9. $g(\mathbf{r})$ parallel and perpendicular to the director. In the left-hand figure, we show $g(\mathbf{r})$ along two paths for $\rho' = 1$ and a discotic orientation of $\tau = -0.4$. The solid line is the isotropic-phase pair correlation at $\rho' = 1$, and the dot-dashed line (which lies above it) is the pair correlation along the \hat{z} axis. The dashed line shows the pair correlation along a lateral axis, \hat{x} . The correlation is much shorter ranged in the \hat{z} direction, lateral to the imposed (discotic) order. The opposite obtains in the right-hand figure, where a comparable nematic ordering is selected, $\tau = 0.8$. Again, the pair correlation is much shorter ranged lateral to the imposed (nematic) ordering, and $g(\mathbf{r})$ orthogonal to the nematic director is also below its isotropic analog for this case.

in extent along the director than perpendicular to it, consistent with the results of Fig. 8. The fluid is more liquidlike along the nematic director (when $\tau > 0$), and more characteristic of a dense melt perpendicular to the director. Figure 9 shows examples of $g(\mathbf{r})$ along the \hat{x} and \hat{z} axes based on Eq. (40). Clearly, $g(\mathbf{r} = z\hat{z})$ grows more slowly than $g(\mathbf{r} = x\hat{x})$, and at $\rho' = 1.0$ the characteristic solvation shells of the isotropic high-density fluid are clearly visible in the perpendicular directions, and are becoming visible in the parallel direction, as well. The relationship of the isotropic $g(\mathbf{r})$ to its anisotropic analog is complicated. The nematic example in Fig. 9 is for a strong degree of alignment: $\tau = 0.5$, $g(\mathbf{r} = x\hat{x}) \approx g(\mathbf{r})$, and for $0 < \tau < 0.5$, $g(\mathbf{r})$ in the perpendicular direction exceeds its isotropic analog. This complex ρ' and τ -dependent relation is discussed further below (see Fig. 11).

It is important to note that while $g(\mathbf{r})$ as shown in Fig. 1 [based on a numerical solution to the transcendental Eq. (12)] is positive definite, the g 's we examine here are based on the approximate solution, Eq. (40), and hence there is a small region near $\mathbf{r} = 0$ where the pair correlation is slightly negative. Nevertheless, it is possible to define the "contact value" of the correlation function by evaluating $g(\mathbf{r})$ with $|\mathbf{r}| = d$. The contact value changes continuously in going from the \hat{z} to the \hat{x} directions, and is of dynamical significance as it controls the rate of local interchain collisions between monomer pairs.²⁶

Figure 10 shows the results for the contact value in the perpendicular and parallel directions as a function of ρ' for a range of discotic and nematic values of τ . In the parallel case

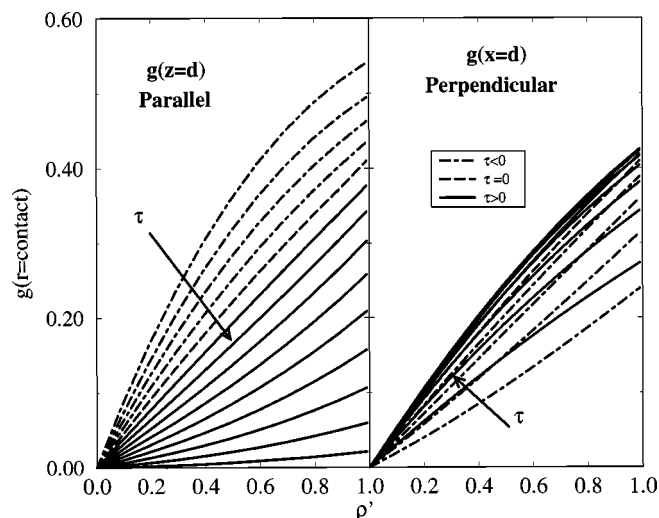


FIG. 10. Anisotropic contact value of the pair correlation. On the left, we show the longitudinal contact value, $g_z \equiv g(\mathbf{r} = z\hat{z})$. g_z monotonically decreases as τ is increased from $\tau = -0.4, \dots, 0.9$ at each value of ρ' . The transverse contact value, $g_\perp \equiv g(\mathbf{r} = x\hat{x})$, has a much more complicated behavior. g_\perp increases with ρ' at fixed τ , just as g_z , but its dependence on τ is nonmonotonic, eventually falling below the isotropic phase contact value even in the extremely discotic, $\tau = -0.4$, configuration.

[$g(\mathbf{r} = d\hat{z})$] the contact value rises monotonically as density increases, and falls monotonically as τ is increased from -0.4 up to 0.9 . The perpendicular contact value, however, displays a very complicated behavior, summarized for two density cases in Fig. 11. In the parallel case, we see a monotonic response, that is, the contact value along the director falls continuously as τ is increased. The perpendicular contact value, however, rises and then falls as τ varies from the discotic to nematic alignments. Generally, the parallel (perpendicular) contact value is much larger than the perpendicular (parallel) contact value at $\tau \rightarrow 1$ ($\tau \rightarrow -1/2$). This is further evidence that the oriented liquid behaves more liquidlike along the established order, and more concentrated laterally.

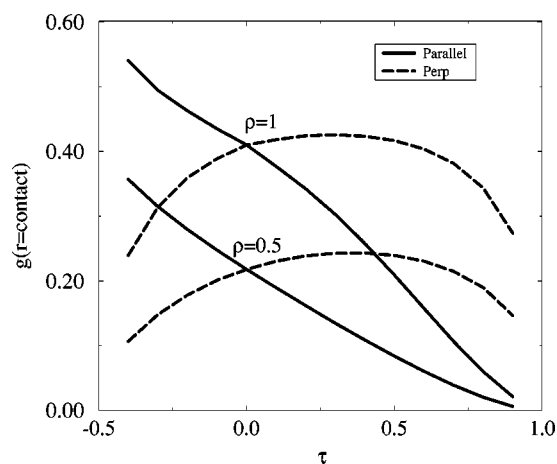


FIG. 11. τ dependence of the longitudinal and transverse contact values of the pair correlation for $\rho' = 1.0$ and $\rho' = 0.5$. The longitudinal (or parallel) contact values is shown as the solid curve, and the transverse (or perpendicular) as the dashed. The longitudinal contact value decreases steadily as τ increases from negative (discotic) to positive (nematic) values, while the transverse value increases and then decreases.

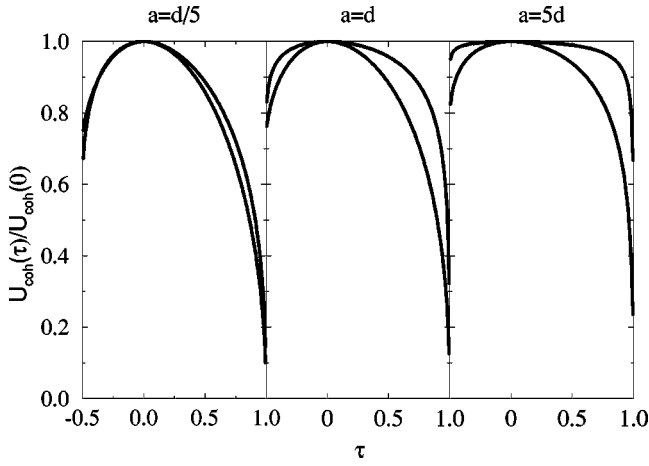


FIG. 12. Scaled cohesive energy, $U_{\text{coh}}(\tau)/U_{\text{coh}}(\tau=0)$, as a function of alignment for various ranges of the attractive potential, $a/d=1/5, 1, 5$. In each case, $\rho'=0.1$ and $\rho'=1.0$ are shown, with intermediate ρ' curves falling between the two cases shown. The cohesion is uniformly smaller for $\rho'=0.1$. When $a \gg d$, the scaled cohesion becomes less sensitive to τ in the vicinity of $\tau=0$ at large density, in keeping with a mean-field treatment of attractions.

An immediate application of this anisotropic structure is to calculate the effect on the *cohesive* energy of an oriented liquid. We take the attractive monomer–monomer potential to be a simple spherically symmetric Yukawa form

$$v(\mathbf{r}) = v(|\mathbf{r}|) = -\frac{v_o e^{-r/a}}{r/a}, \quad (50)$$

with a magnitude $v_o > 0$, and a spatial range of a . Based on the standard high temperature, or mean-field, approximation (HTA) that assumes local liquid structure is determined by the repulsive, athermal excluded volume interaction,^{19,20} the cohesive energy per monomer is

$$U_{\text{coh}} = \rho \int d\mathbf{r} v(r) g(\mathbf{r}; \tau). \quad (51)$$

Even though the monomer–monomer interaction is manifestly isotropic, U_{coh} depends on τ directly through the athermal liquid structure, $g(\mathbf{r}; \tau)$. We anticipate that as $|\tau|$ increases, the number of monomers within a distance a of a test monomer will decrease monotonically. Each panel in Fig. 12 shows the cohesion relative to its isotropic-phase value [based on a numerical, not interpolated, solution of Eqs. (12) and (36)], as the *range* of the interaction is tuned from a large to a small value. For $a \gg d$, it is apparent that the cohesion becomes a less sensitive function of τ . Indeed, we anticipate a literal “mean-field” or “Kac potential” limit in which $a \rightarrow \infty$ (and $v_o \rightarrow 0$). In this case, there can be *no* τ -dependence in U_{coh} . Likewise, for $a \ll d$ the τ dependence of the cohesion is enhanced.

It is instructive to analytically examine the small τ behavior of U_{coh} scaled by its isotropic value. For convenience, we restrict our attention to $\rho'=1$, that is the maximum density, close-packed state of isotropic chains. At $\rho'=1$,

$$\xi' \sim \frac{6\tau}{\pi\sqrt{5}} + O[\tau^2], \quad (52)$$

as can be verified by substituting this relation into Eq. (36). When this result is used in calculating U_{coh} we obtain

$$\frac{U_{\text{coh}}(\tau)}{U_{\text{coh}}(\tau=0)} = 1 - \left(\frac{3d^2 + 4\pi^2 a^2}{5\pi^2 a^2} + \frac{8\pi a}{5(d \arctan[2\pi a/d] - 2\pi a)} \right) \tau^2 + O[\tau^3]. \quad (53)$$

For extremely short ranged interactions ($a \ll d$),

$$\frac{U_{\text{coh}}(\tau)}{U_{\text{coh}}(\tau=0)} = 1 - \left(\frac{16}{25} - \frac{576\pi^2 a^2}{875d^2} \right) \tau^2 + O[\tau^3]. \quad (54)$$

On the other hand, when $d \ll a$

$$\frac{U_{\text{coh}}(\tau)}{U_{\text{coh}}(\tau=0)} = 1 - \frac{d}{5a} \tau^2 + O[\tau^3]. \quad (55)$$

Thus, as is evident in Fig. 12, at the maximal density, longer attractive interaction ranges imply that the anisotropic response to the cohesion becomes “flatter” in τ , that is becomes less sensitive to the anisotropy for small anisotropies. As the range of the interaction shrinks, the liquid structure on the scale of a becomes nontrivial, and the response becomes sharpest.

Qualitatively similar statements hold when ρ' is less than its maximal value. In particular, taking the thread limit

$$\frac{U_{\text{coh}}(\tau)}{U_{\text{coh}}(\tau=0)} = 1 - \left[\frac{3(9 + 4\pi\rho a\sigma_o^2)}{5(3 + \pi\rho a\sigma_o^2)^2} \right] \tau^2 + O[\tau^3]. \quad (56)$$

Thus, when $a \ll \sigma_o$ the relative cohesion decreases with $\tau \neq 0$

$$\frac{U_{\text{coh}}(\tau)}{U_{\text{coh}}(\tau=0)} = 1 - \left(\frac{3}{5} - \frac{2\pi\rho a\sigma_o^2}{15} \right) \tau^2 + O[\tau^3]. \quad (57)$$

While this expression displays more sensitivity to a than the $\rho'=1$ situation, the response of the cohesion is strongest to τ for $a \rightarrow 0$, as before. In the mean-field limit, $a \gg \sigma_o$, the relative cohesion takes the form

$$\frac{U_{\text{coh}}(\tau)}{U_{\text{coh}}(\tau=0)} = 1 - \frac{12}{5\pi\rho a\sigma_o^2} \tau^2 + O[\tau^3]. \quad (58)$$

The full density dependence of the relative cohesion is bracketed by these thread expressions (valid at small d , or equivalently, small ρ') and by the $\rho'=1$ expressions above. We discuss the implications for these results on the phase stability of confined polymer blends below.

V. DISCUSSION

Our treatment of anisotropy can be extended to a variety of extended objects. For macromolecules characterized by a self-similarity mass fractal dimension D_f , embedded in a D_s -dimensional space, the following ω_{frac} ³⁴ describes the isotropic phase:

$$\omega_{\text{frac}}(q) = N[1 + c_1 q^2 R_g^2]^{-D_f/2}, \quad (59)$$

where the fractal dimension is related to the radius of gyration through a power law

$$R_g = c_2 N^{1/D_f}, \quad (60)$$

and c_1 and c_2 are known constants.³⁴ This form for ω_{frac} is essentially an interpolation between the exact small q behavior ($qR_g \ll 1$), and the large q behavior ($qR_g \gg 1$) that has $\omega_{\text{frac}} \approx q^{-D_f}$ appropriate to the self-similar scattering from a fractal of dimension D_f . The isotropic Lorentzian form for $\omega(\mathbf{q})$ in Eq. (1) is thus ω_{frac} with $D_f = 2$.

The spatial dimension enters explicitly in executing the core exclusion condition

$$\int \frac{d^D_s q}{(2\pi)^{D_s}} h(\mathbf{q}) = -1. \quad (61)$$

As previously shown,³⁴ if $D_f < D_s/2$, then an ultraviolet divergence in Eq. (61) requires the presence of a high-wave vector cutoff, and for such systems there is no analog of the thread theory. That is, the monomer-scale length, d , is always a relevant length scale, and there is no universal limit corresponding to semidilute polymer solutions. Clearly, random walk polymers in three dimensions have a universal regime, while rodlike polymers, $D_f = 1$, in three dimensions do not. Random walks confined to an ideal surface ($D_f = D_s = 2$), or fluctuating globules ($D_s = D_f = 3$), can be easily handled through the use of ω_{frac} .³⁴ Here, d is irrelevant at small densities, and there is an interesting universal regime. Such compact macromolecules cannot, however, significantly interpenetrate (since $D_f = D_s$).

The anisotropy of the objects can be addressed through the transformation

$$\mathbf{q} \cdot \mathbf{q} R_g^2 \rightarrow R_z^2 q_z^2 + R_\perp^2 q_\perp^2, \quad (62)$$

in the definition of ω_{frac} . As an example of the power of the formalism, ω_{frac} for long, thin rods ($D_f = 1$) in three-dimensional space can be used to capture all the important qualitative features of the Onsager treatment^{1,2} of the nematic phase, as we show in the following companion paper.²³

Within a thermodynamic perturbation approach (HTA at the level of the solution free energy rather than the compressibility) it is possible to determine the effect of weak attractions on the equation of state and the compressibility, as previously worked out for the isotropic phase of string model polymers.³⁰ The reference, athermal free energy can be derived from our compressibility route charging, to which can be added the cohesive energy, U_{coh} . Such a treatment, when coupled with a theory of the isotropic–nematic transition of flexible polymers, allows a unified treatment of thermotropic and lyotropic transitions, in either an isochoric ($\rho' = \text{const}$) or isobaric ensemble (most clearly relevant to experiment).³⁵

As a quick application of this thermodynamic perturbation approach we consider a structurally symmetric polymer blend ($\sigma_A = \sigma_B \equiv \sigma_o$) of long polymers ($N \rightarrow \infty$) confined in a thin (less than or on the order of R_z) film of thickness, H . We expect that confinement will lead to alignment of the chains, and hence a decrease in the cohesion of the film. The degree of confinement, H/R_z imposes a τ on the system which may be naively estimated for small τ as:

$$\tau(H) = \frac{H - R_z}{H}. \quad (63)$$

Thus, a 10% compression induces $\tau = -0.1$, that is 20% discotic alignment. Using Eq. (55) indicates that the cohesive contribution to the free energy decreases relative to the unconfined blend by $\approx (\frac{1}{500})(d/a) \sim \frac{1}{125}$ if we choose $d = 2a$, as is appropriate for modeling a Lennard-Jones attraction with a Yukawa.¹⁹ Since the critical temperature of the melt blend in the bulk is proportional to $N|U_{\text{coh}}|$, lowering $|U_{\text{coh}}|$ by enforcing $\tau < 0$ will likewise lower the critical temperature, stabilizing the homogeneous mixture. If the critical temperature of the blend is in the neighborhood of room temperature, 300 °K, then the fractional change in the critical temperature that accompanies a 10% confinement is on the order of 2–3 °K, clearly a measurable effect that will grow in importance as H is lowered. A similar argument can be applied to the thermodynamics of weakly sheared polymer blends.⁴

VI. CONCLUSION

We have extended the range of applicability the PRISM liquid state formalism to include homogeneous systems characterized by global anisotropy, and have presented a detailed exhibition of the theory when applied to *nematic* and *discotic* configurations of flexible polymers. In the liquid crystalline phases, the compressibility increases with increasing alignment, and therefore, the repulsive pressure decreases. We anticipate that this lowering of excluded-volume interactions will act to stabilize liquid crystallinity in equilibrium thermodynamics. All structural characteristics of the aligned fluid are anisotropic as well, including the screening of collective density fluctuations and the contact value of the pair correlation function. The theory may be equally well applied to describe some aspects of the thermodynamics of confined blends and provides needed structural input to mode coupling theories of the dynamics of anisotropic polymer fluids.²² Generalization to include more chemical realism (e.g., backbone stiffness) in the single chain model, and the full wavevector dependence of the direct correlation function, requires additional numerical effort but is straightforward.

ACKNOWLEDGMENTS

This work was performed at the University of Illinois at Urbana-Champaign and was supported by the U.S. DOE Division of Materials Science Grant No. DEFG02-96 ER45539 through the University of Illinois Materials Research Laboratory.

¹D. Frenkel, Les Houches, Session L1, 1989 *Liquids, Freezing, and Glass Transition*, edited by J. P. Hansen, D. Levesque, and J. Zinn-Justin (Elsevier, B. V., 1991); G. J. Vroege and H. N. W. Lekkerkerker Rep. Prog. Phys. **55**, 1241 (1992); P. G. deGennes, *Physics of Liquid Crystals* (Oxford University Press, Oxford, 1974).

²L. Onsager, Ann. N.Y. Acad. Sci. **51**, 627 (1949).

³L. A. Utracki, *Polymer Blends and Alloys* (Hanser, New York, 1989).

⁴W. Bruns and W. Carl, *Macromolecules* **26**, 557 (1993).

⁵E. Helfand and G. H. Fredrickson, Phys. Rev. Lett. **62**, 2468 (1989); H. P. Wittmann and G. H. Fredrickson, J. Phys. I **4**, 1791 (1994).

⁶A. Onuki, Phys. Rev. Lett. **62**, 2472 (1989).

- ⁷T. Sun, A. C. Balazs, and D. Jasnow, *Phys. Rev. E* **59**, 603 (1999).
- ⁸A. Abe, E. Iizumi, and N. Kimura, *Liq. Cryst.* **16**, 655 (1994); S. F. Edwards and T. C. B. McLeish, *J. Chem. Phys.* **92**, 6855 (1990).
- ⁹G. Fleer, M. A. Cohen-Stuart, J. M. H. M. Scheutjens, T. Cosgrove, and B. Vincent, *Polymers at Interfaces* (Chapman and Hall, London, 1993).
- ¹⁰S. Granick, *Phys. Today* **52**, 26 (1999).
- ¹¹M. N. Matrosova, L. V. Mochalova, V. P. Marinina, N. E. Byramova, and N. V. Bovin, *FEBS Lett.* **272**, 209 (1990).
- ¹²W. W. Maurer, F. S. Bates, T. P. Lodge, K. Almdal, K. Mortensen, and G. H. Fredrickson, *J. Chem. Phys.* **108**, 2989 (1998).
- ¹³J. C. Chung, D. J. Gross, J. L. Thomas, D. A. Tirrell, and L. R. Opsahl-Ong, *Macromolecules* **29**, 4636 (1996).
- ¹⁴A. Srivastava and K. B. Eisenthal, *Chem. Phys. Lett.* **292**, 345 (1998).
- ¹⁵D. Gersappe, W. Li, and A. C. Balazs, *J. Chem. Phys.* **99**, 7209 (1993).
- ¹⁶J. A. Forrest, K. Dalnoki-Veress, and J. R. Dutcher, *Phys. Rev. E* **56**, 5705 (1997).
- ¹⁷L. Sung, A. Karim, J. F. Douglas, and C. C. Han, *Phys. Rev. Lett.* **76**, 4368 (1996).
- ¹⁸G. T. Pickett and K. S. Schweizer, *J. Chem. Phys.* **110**, 6597 (1999).
- ¹⁹For reviews, see K. S. Schweizer and J. G. Curro, *Adv. Chem. Phys.* **98**, 1 (1997); *Adv. Polym. Sci.* **116**, 319 (1994).
- ²⁰D. Chandler, in *Studies in Statistical Mechanics, Vol. VIII*, edited by E. W. Montroll and J. L. Lebowitz (North-Holland, Amsterdam, 1982), p. 274.
- ²¹K. S. Schweizer and J. G. Curro, *Macromolecules* **21**, 3070, 3082 (1988); *Chem. Phys.* **149**, 105 (1990).
- ²²K. S. Schweizer, M. Fuchs, G. Szamel, M. Guenza, and H. Tang, *Macromol. Theory Simul.* **6**, 1037 (1997).
- ²³G. T. Pickett and K. S. Schweizer, *J. Chem. Phys.* **112**, 4881 (2000), following paper.
- ²⁴C. M. Marques and G. H. Fredrickson, *J. Phys. II* **7**, 1805 (1997).
- ²⁵P. G. deGennes, *Scaling Concepts in Polymer Physics* (Cornell University Press, Ithaca, 1979).
- ²⁶J. P. Hansen and I. R. McDonald, *Theory of Simple Liquids* (Academic, London, 1986).
- ²⁷Interestingly, the thread formulation of PRISM can also be derived through examining the exclusion of a harmonically fluctuating collective density field from the one-dimensional manifold describing the backbone trajectory of a flexible polymer, as in D. Chandler, *Phys. Rev. E* **48**, 2898 (1993).
- ²⁸M. Fuchs, *Z. Phys. B* **103**, 521 (1997).
- ²⁹The dilute regime is defined so that individual polymer chains in their native configurations do not approach each other in space. That is, $\rho < \rho^* \approx N/R_g^3$, as the typical volume occupied by the N monomers on an isolated coil is $4\pi R_g^3/3$. When $\rho \gg \rho^*$, but the concentration of monomers is still very small, $\rho \ll \sigma_o^{-3}$, the polymers are strongly entwined, and such a "semidilute" solution is governed by the collective "universal" properties of the entangled chains.
- ³⁰A. P. Chatterjee and K. S. Schweizer, *Macromolecules* **31**, 2353 (1998).
- ³¹In a truly incompressible fluid one does expect the contact value of the intermolecular pair correlation function, $g(r=d)$, will diverge at random close packing. This behavior is found from computer simulations of the hard-sphere fluid as the random close packing density is approached. However, such a divergence is not captured by approximate integral equation theory (PY for hard spheres), and is also not expected to be properly described by PRISM theory for polymer liquids especially based on the highly coarse-grained chain model studied in this paper.
- ³²There is clear experimental evidence that for the nematic phases of side-chain liquid crystal polymers, the overall radius of gyration of the chains is unchanged at the nematic-isotropic transition, and into the ordered phase as well. Modeling the chain statistics through Eq. (23) is thus more than a simplifying assumption. The exact relationship between side-chain and main chain LCP's in our theory is a matter for further study. See R. G. Kirste and H. G. Ohm, *Makromol. Chem., Rapid Commun.* **6**, 179 (1985).
- ³³To roughly estimate the behavior of S_o for a finite molecular weight, one simply needs to draw a horizontal line at N , as the growth of the compressibility must be cutoff smoothly at that value.
- ³⁴M. Fuchs and K. S. Schweizer, *J. Chem. Phys.* **106**, 347 (1997).
- ³⁵G. T. Pickett and K. S. Schweizer (to be published).